

Developing Mg-Zn-Fish Bone Derived Hydroxyapatite Composites for Biomedical Applications: *In vitro* Degradation Studies

Manoj Kumar Elipey ¹, Talakayala Sunil Kumar ², Ravikumar Dumpala ³, Ratna Sunil Bradagunta ^{4,*}

¹ Department of Mechanical Engineering, Vardhaman College of Engineering, Shamshabad 501218, India; emanoj2000@gmail.com (M.K.E);

² Department of Mechanical Engineering, Geethanjali Institute of Science & Technology, Gangavaram 524137, India; suneilkumart@gmail.com (T.S.K.);

³ Department of Mechanical Engineering, Visvesvaraya National Institute of Technology, Nagpur 440010, India; ravikumardumpala@mec.vnit.ac.in (R.K.D.);

⁴ Department of Mechanical Engineering, Bapatla Engineering College, Bapatla 522101, India; bratnasunil@gmail.com (B.R.S.);

* Correspondence: bratnasunil@gmail.com (B.R.S.);

Scopus Author ID 35410353400

Received: 16.09.2021; Revised: 15.10.2021; Accepted: 18.10.2021; Published: 21.11.2021

Abstract: The study of magnesium (Mg) based biomaterials has emerged as a potential research area in recent times. Controlling the rapid corrosion and improving the implant-tissue interface kinetics for better tissue regeneration are the prime interests behind developing novel Mg-based composites. In the current work, the metal matrix composites of Mg-Zn, dispersed with nano-hydroxyapatite derived from fish bones (fHA), were produced by powder metallurgy route. The powders were mixed with the help of ball milling in the presence of ethanol and then sintered at 440 °C. From the microstructural studies, micro-lamellar morphology was noticed for the sintered compacts due to the flake-like morphology of the milled powders. The sintered compacts were then subjected to *in vitro* biodegradation studies in simulated conditions for one week. From the results, the presence of fHA was found to be highly influential in increasing the rate of mineral deposition on the surface of the composites. These higher mineral depositions protected the surface of the composites from further degradation. The results demonstrate that adding fHA to Mg accelerates biomineralization and controls degradation, leading to better implant-tissue interactions.

Keywords: fish bones; calcium phases; degradable implants; surface degradation; biomineralization.

© 2021 by the authors. This article is an open-access article distributed under the terms and conditions of the Creative Commons Attribution (CC BY) license (<https://creativecommons.org/licenses/by/4.0/>).

1. Introduction

Developing composite materials by combining different phases helps material scientists to produce modern materials with hybrid properties [1]. Metals exhibit superior mechanical properties required to manufacture load-bearing medical implants compared with polymers and ceramic materials. On the other hand, ceramic materials possess excellent biocompatibility. Calcium-based ceramics exhibit bioactive nature and can develop strong bonding with the tissue [2]. Hence, developing composites by incorporating bioactive ceramic phases helps to produce novel biomaterials with desired properties [3,4]. For the past two decades, significant interest has been shown in developing magnesium (Mg) based implants for orthopedic applications due to excellent bio-properties [5-8]. The main objective of the research groups

across the globe on developing Mg implants is to control the rapid degradation and to enhance the tissue bonding at the implant interface [9-12]. In this context, incorporating bioactive ceramic phases into Mg-based materials to develop composites is a promising strategy [13-16].

Hydroxyapatite (HA) is a ceramic phase of calcium (Ca) and phosphorous (P) that can be seen in higher fractions in the bones of mammals. Human bones also contain HA crystals at the nano-level and collagen and other growth factors [17]. HA is used as bone filling material, medium for targeted drug delivery, and to manufacture dental implants in biomedical applications [18,19]. HA can be obtained by natural resources or can be synthesized in the laboratory. For naturally derived HA, fish bones, scalps, sea corals, eggshells, etc., can be used as precursors [20-24]. Synthetically produced HA is obtained by using specific chemicals such as calcium hydroxide, calcium nitrates, ammonium phosphates, etc., in appropriate proportions by following various protocols as reported in the literature [25-28]. HA derived from natural resources contains additional ions. In our earlier work, nano-HA was successfully synthesized from fish bones (*rohio*), and the presence of zinc was noticed in addition to calcium and phosphorous [29].

Ball milling is a powder processing technique in which powders are uniformly mixed and repeatedly subjected to the collision between the balls. Prolonged milling times also help to reduce the particle size [30]. Developing composites by powder metallurgy needs appropriate blending of the powders of the constituting phases. The powder blends are then compacted by applying pressure and heat in a protected environment or vacuum with a proper heating rate. This process in powder metallurgy is known as sintering. Since the process is carried out in solid-state, the issues associated with the liquid state, such as oxidation, formation of new phases, and decomposition of existing phases, can be eliminated. Other processes such as powder mixing and hot extrusion, melting and extrusion, friction stir processing, spark plasma sintering can be seen in the literature in developing composites of Mg for medical implant applications [31-35]. Being an essential micronutrient, zinc (Zn) is required for several metabolic activities in the human body. Mg-Zn alloys were demonstrated as one of the promising Mg alloy systems for biomedical applications [12]. Information on using ion-containing HA, such as naturally derived HA, as a reinforcing material to develop Mg-based implants is insufficient in the reported scientific literature. Hence in the present work, fish bone-derived nano-HA (fHA) was dispersed into pure Mg using ball milling, and the milled powders were consolidated by sintering at 440 °C. The effect of adding fHA on biomineralization was assessed by conducting *in vitro* bioactivity studies in simulated conditions.

2. Materials and Methods

Pure Mg powder (99.5 % purity, Merk, India) and pure Zn powder (99.9 % purity, Quality Traders, Guntur, India) were procured and used in the present work. Fish bone-derived hydroxyapatite (fHA) was produced in the laboratory from fish (*Rohio*) bones. The procedure to synthesize nano-HA from fish bones can be referred to in our earlier report [29]. In the present composition, the Zn fraction was limited to 1%, as the solubility limit of Zn element (solute) into Mg lattice (solvent) is less than 1% at the room temperature [28, 36]. Excess amount of Zn leads to develop MgZn intermetallics, which increase the degradation rate due to bio-corrosion [37,38]. Different percentages of fHA (1 and 2 wt.%) were added to Mg-1%Zn, and composites were developed. A higher fraction of reinforcements in the Mg matrix accelerates the degradation rate in the corroding environment. Hence, the addition of fHA was

limited to lower amounts (1 and 2%). The powders with appropriate weights were milled by using a planetary ball mill for 20 h. Tungsten carbide (WC) vials and balls were used for the milling process. Total balls weight to milling powder weight ratio was maintained as 20:1. Ethyl alcohol was filled in the vial before milling about covering the powders completely. After ball milling, the collected powders were dried and compacted in a cylindrical die of 10 mm diameter using a hydraulic press. X-ray diffraction (XRD) studies (using $\text{CuK}\alpha$) have been carried out between 20 to 80 ° for all the powder samples with a scanning step size of 0.1. The compacted pellets were then placed in a furnace, and sintering was done at 440 °C in the presence of Argon gas. Heating of 5 °C/min was adopted, and 1 h of soaking time was given to stabilize the temperature throughout the samples. Then the samples were furnace cooled and named as Mg-Zn, Mg-Zn-1fHA, and Mg-Zn-2fHA for 0, 1, and 2 percent of added fHA, respectively. Figure 1 shows the sintering cycle and typical photograph of Mg-Zn-2fHA composite.

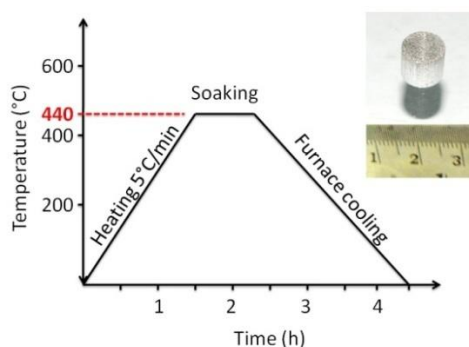


Figure 1. The heating, soaking, and cooling cycle adopted in the current work (inset: typical photograph of sintered Mg-Zn-2fHA composite).

A standard metallurgical procedure was adopted to prepare the samples for polishing [35]. After etching with a picric acid agent, microstructures were recorded using an optical microscope (Leica, Germany). Simulated physiological test conditions were provided by preparing a solution with a similar ion concentration of human blood plasma in the laboratory. The protocol for preparing the simulated body fluid (SBF) and the lab grade chemicals and their relative weights can be referred elsewhere [39]. The samples of size 10 mm diameter and 5 mm height were prepared, polished, and cleaned for immersion studies. While preparing the SBF, the appropriate amount of ammonia was added to maintain a pH of ~ 7.4. Each container was filled with 50 ml of SBF, and then the samples were placed in the containers. The weights of the samples were recorded before and after the immersion test to calculate the weight loss after one day and one week. Usually, for Mg alloys, rapid degradation is observed during the initial hours of degradation. Understanding the degradation behavior of Mg-based material during initial hours is crucial in developing Mg-based implants. Hence, immersion studies have been conducted for one week. The pH of the solution was recorded every 12 h for all the samples. After one day and one week, all the samples were collected and placed in a container of distilled water (for 30 min) and then dried in an open atmosphere. The morphologies of the powders and the immersed samples were analyzed by scanning electron microscope (SEM, TESCON, Czech Republic), and energy-dispersive X-ray spectroscopy (EDS) was also carried out. The samples after the immersion test were placed in chromate aqua solution (180 g of CrO_3 has been added to 100 ml of boiling water) to dissolve the corrosion products produced during the degradation process. After 30 min, the corrosion products from the surface of the immersion samples were observed as completely dissolved in the chromate aqua solution. Then the weight

of the degraded samples was measured to assess the weight loss (mg/cm^2). The difference between the weight of the samples before immersion and after dissolving the corrosion products was obtained and divided by the surface area of the samples.

3. Results and Discussion

The Mg powders used to produce the composites, as shown in Figure 2(a), have an average size of $172 \pm 4.1 \mu\text{m}$. The corresponding EDS analysis (Figure 2 (b)) confirms that the particles are free from impurities. Bright-field TEM image (Figure 2 (c)) of nano-hydroxyapatite produced from fish bones (fHA) shows equiaxed morphology with an average size of $\sim 75 \text{ nm}$. The selective area electron diffraction (SAED) pattern of produced fHA shows spots arranged in ring pattern (Figure 2(d)) which confirms the nano-dimension of the produced fHA. Ball milling for lower periods helps to mix the powders appropriately. If milling time is increased to higher periods, cold welding and fracturing of particles, size reduction, and uniform distribution of reinforcing phases into the matrix particles can be achieved [40].

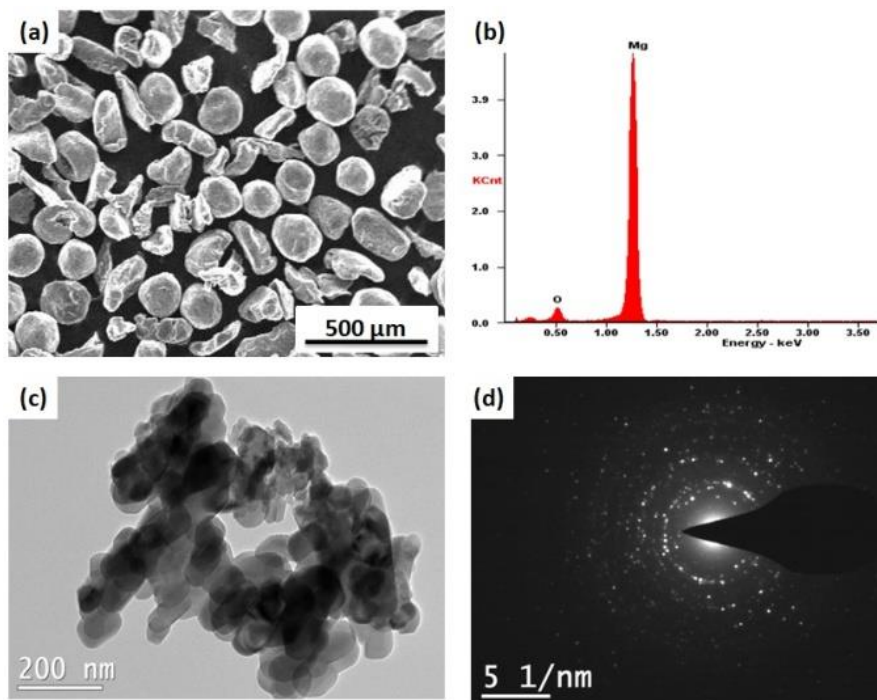


Figure 2. (a) SEM images of pure Mg powders and (b) EDS analysis, (c) bright-field transmission electron microscope image of fHA, and (d) corresponding SAED pattern.

Figure 3 shows the morphologies of ball-milled powders after 20 h of milling. Usually, particle size is greatly reduced after such long milling periods, as reported in the literature [40]. From the results, it can be learned that pure Mg, Mg-Zn-1fHA, and Mg-Zn-2fHA powders have transformed into flake-like morphology. Since Mg is soft, the particles were subjected to plastic deformation and deformed as thin flakes due to milling, and the thickness was significantly decreased. The size distribution of Mg particles after milling was found to be in a wide range between sub-micrometers to around $50 \mu\text{m}$. The corresponding EDS analysis of the composites (Fig 3 (d) and (f)) shows the presence of calcium and phosphorous, in addition to magnesium, oxygen, and zinc in the composites due to the added nano-fHA.

Figure 4 presents the XRD plots of pure Mg, fHA, and ball-milled powders. Peaks corresponding to Pure Mg and fHA were indexed, and the findings support the chemical

composition analysis (Figure 3) that no contamination present in the powders. Interestingly, the relative intensities of peaks of the composite powders after ball milling were observed as changed. The peak intensity of (002) of the composite powders was significantly increased, and other peak intensities were observed as decreased due to ball milling. (002) peak corresponds to the basal plane in *hcp* Mg, and therefore, it can be noted that a preferred orientation has occurred within the particles during the plastic deformation. Obtaining a preferred texture in Mg can alter biodegradation. It was also reported that the basal-dominated texture influences the electrochemical events at the implant-tissue interface and affects the degradation process [40,41]. Figure 5 shows the microstructure of the sintered samples. Since the Mg particles transformed into thin flakes due to the ball milling process, the resulting solid compacts also exhibited the same morphology for the grains in the sintered samples. These gains are similar to the micro-lamellar structure reported in the literature [42]. A large difference in the length to thickness is the main characteristic of microlamellar grains. Due to the lamellar structure at the microscopic level, the developed composites behave differently compared with the constituting phases. The black regions are the interfaces between the lamellar grains, and the bright regions are the grain interiors (Figure 5). Usually, the reinforcing phase is distributed at the interfaces of the grains in the composites developed through ball milling followed by sintering [30, 42]. Therefore, in the present work, the added fHA crystals are believed to be distributed at the interfaces of the grains.

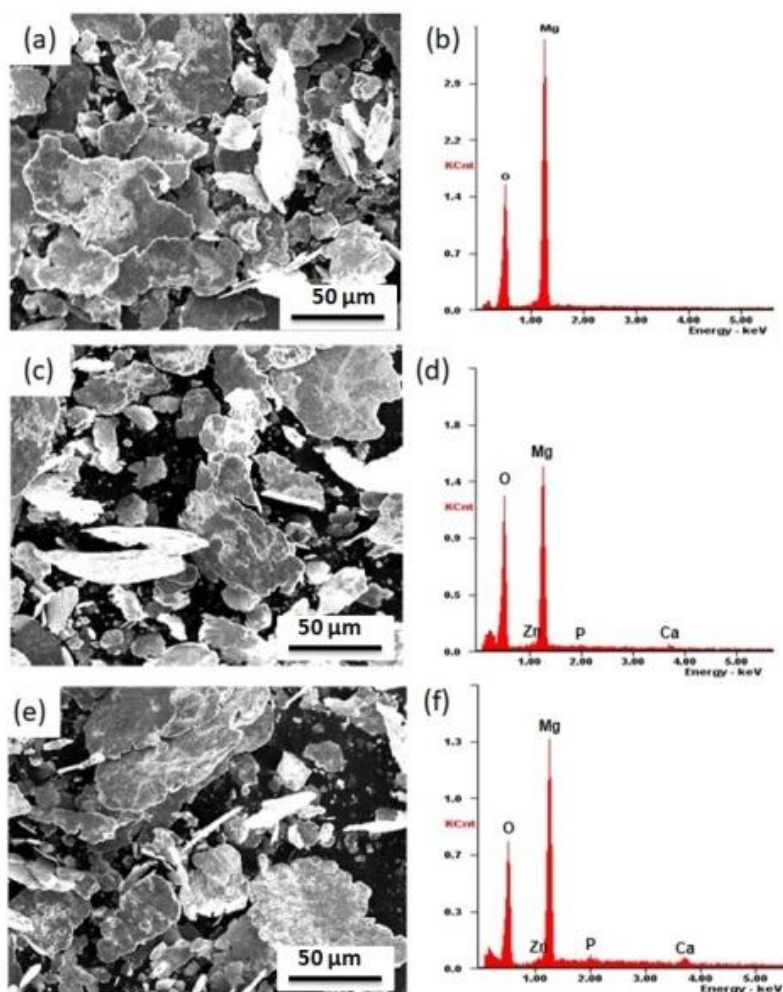


Figure 3. Scanning electron microscope (SEM) images and corresponding EDS analysis of milled powders: (a) and (b) Mg powders, (c) and (d) Mg-Zn-1fHA, (e) and (f) Mg-Zn-2fHA.

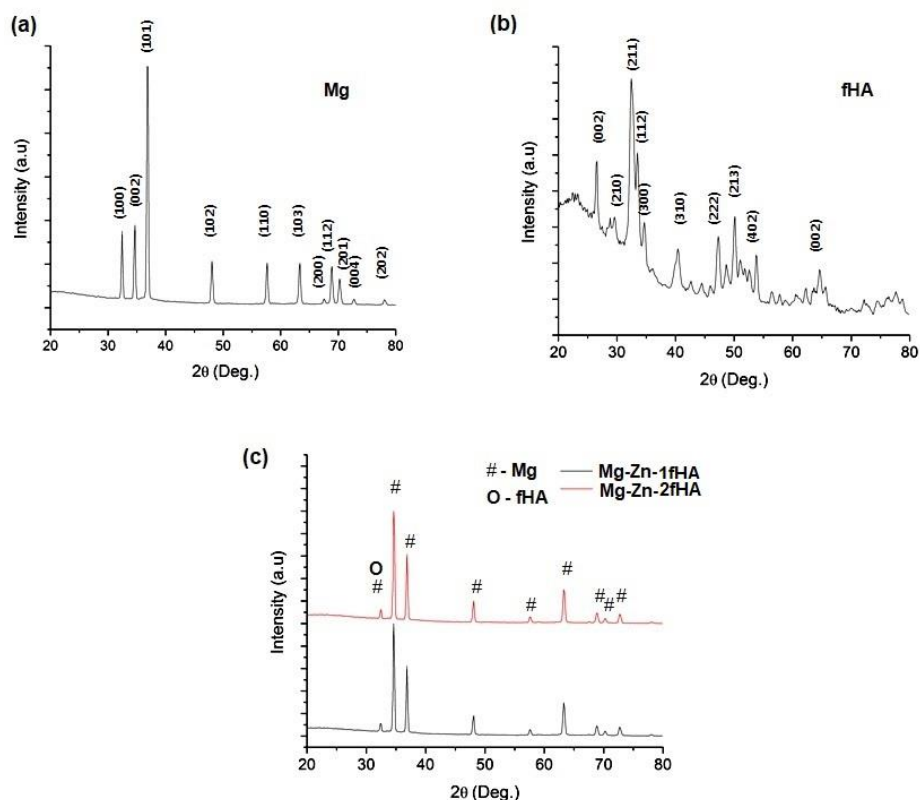


Figure 4. XRD patterns of powders: (a) pure Mg powder, (b) fHA powder, (c) composite powders after ball milling.

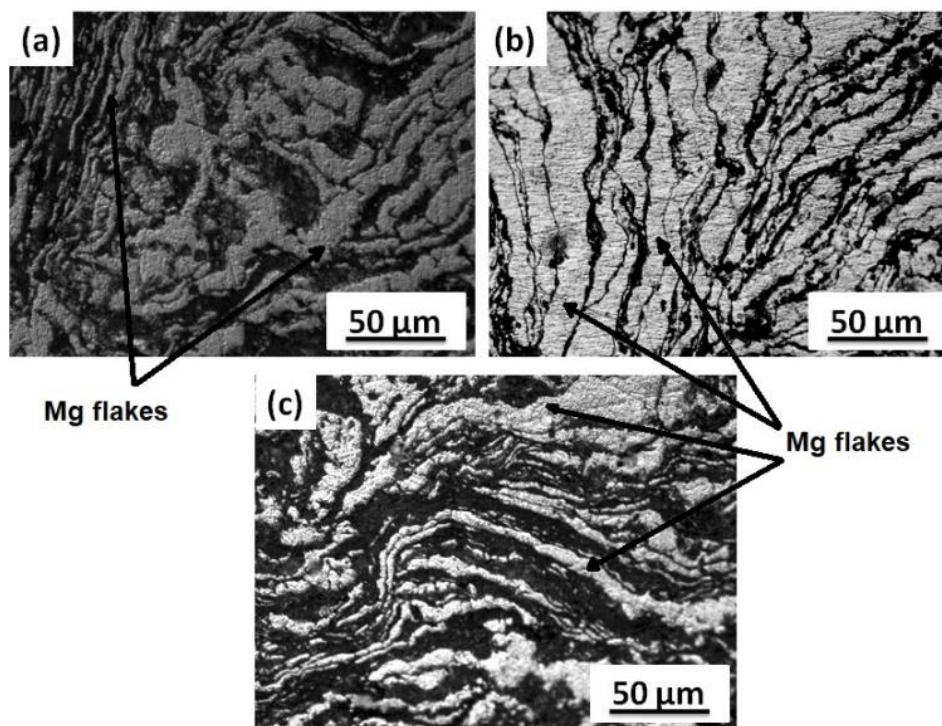


Figure 5. Microstructure of the sintered samples: (a) pure Mg, (b) Mg-Zn-1fHA, and (c) Mg-Zn-2fHA.

Figure 6 presents the morphologies of surface mineral depositions and their corresponding elemental composition obtained from the samples after 72 h of immersion in SBF. It is evident from the deposited phases and the elemental composition that the presence of fHA has a profound effect on increasing the deposition of phases that contain calcium (Ca) and phosphorous (P) as the main constituting elements. A higher level of deposition of Ca/P

on the composites compared with pure Mg suggests an increase in the biomineralization, a process by which mineral depositions are influenced at the implant-tissue interface. Micro-lamellar grain structures with the presence of fHA crystals throughout the composite influenced the biomineralization process. Enhanced mineral deposition helps to lower the degradation process by delaying the dissolution of Mg from the implant. Furthermore, surfaces with higher mineral depositions are favorable for cell adhesion and growth.

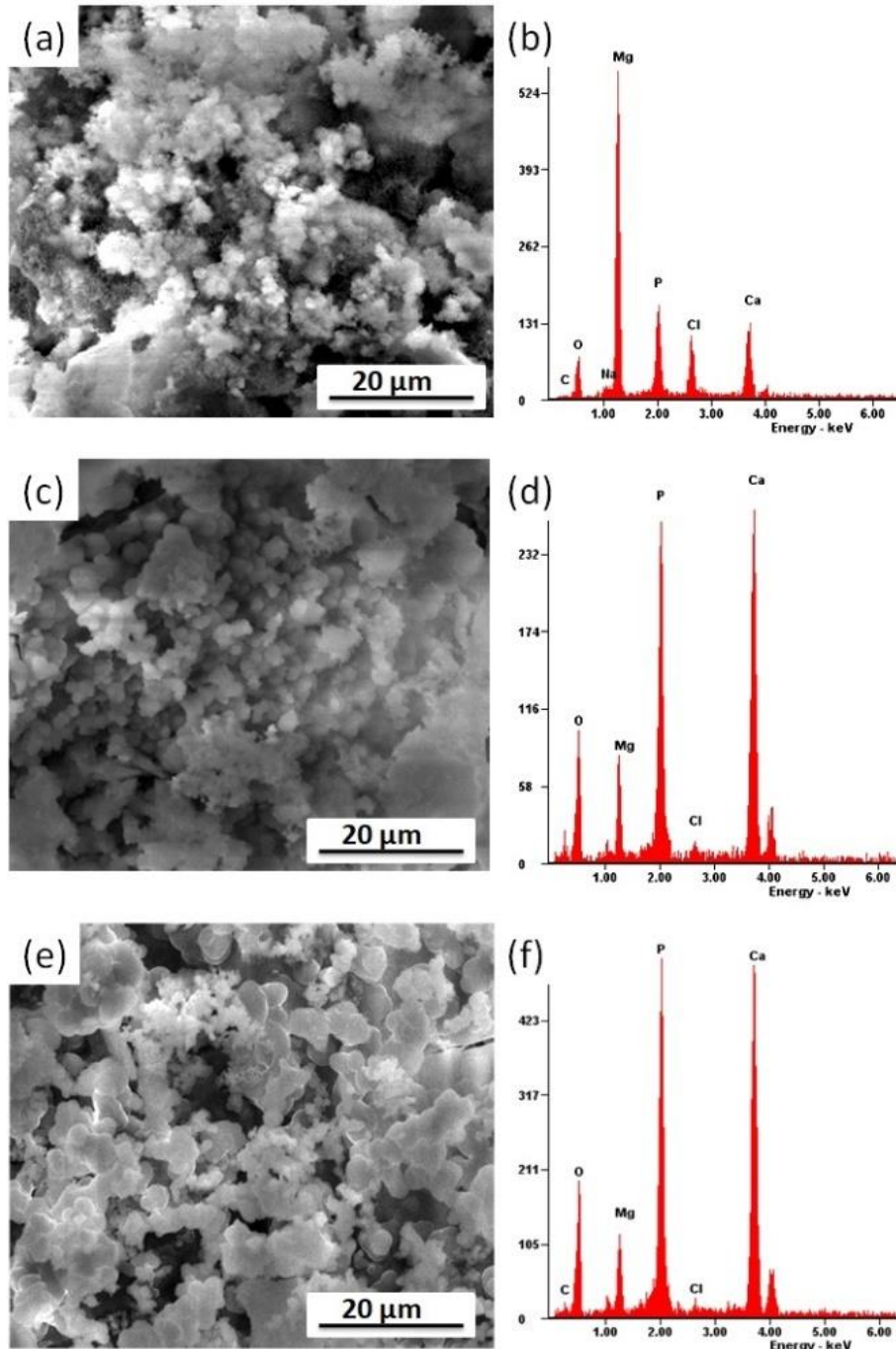


Figure 6. SEM images and chemical composition of the surfaces of the samples after 72 h in SBF: (a) pure Mg, (b) surface EDS analysis, (c) Mg-Zn-1fHA, (d) surface EDS analysis, (e) Mg-Zn-2fHA, and (f) surface EDS analysis.

The corrosion products are completely removed from the surface of the samples by dissolving them in the chromate solution, and the measured weight loss values of the samples are compared in Figure 7. It is observed that with the increased immersion time from 24 h to

72 h, the degradation rate of the samples was increased. Composites exhibited relatively lower weight loss than pure Mg. Within the composites, the sample with 1% HA has shown lower degradation compared with the sample having 2% HA. Both the composites exhibited excellent deposition of mineral phase due to the presence of nano-HA, which accelerated the crystal formation and growth of the Ca/P mineral phase from the SBF. However, the presence of more HA increased the degradation rate. This can be explained by considering the galvanic corrosion due to the contact of different phases with varying electrochemical potentials. The presence of more HA (ceramic phase) in Mg (metallic phase) accelerates galvanic corrosion in the composite. The mineral deposition helped to decrease the degradation due to bio-corrosion. When fHA content was increased to 2% due to the increased galvanic corrosion, the degradation rate was increased compared with 1% fHA composite. However, enhanced mineral deposition has reduced the overall corrosion of both the composites compared with pure Mg.

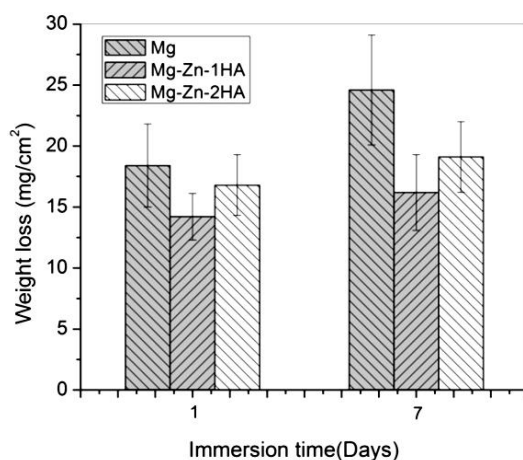


Figure 7. Weight loss measurements of the samples calculated from the immersion studies.

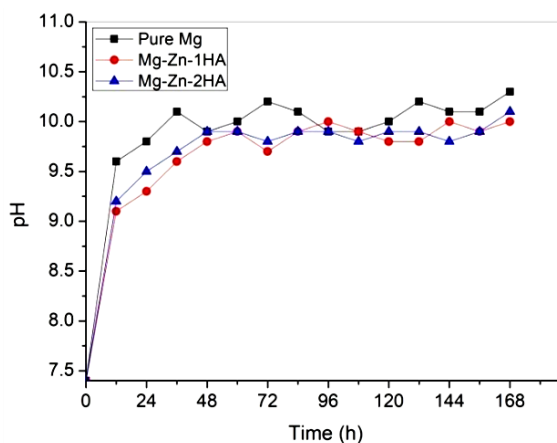


Figure 8. pH variations in the SBF during the immersion period.

Figure 8 shows the pH measurements of the SBF solution for the samples recorded for 7 days. The pH values of the SBF in all the containers were measured and observed as increased due to the nature of aggressive corrosion of Mg during the initial hours of contact with an aqueous solution. During the degradation of Mg in the presence of a physiological environment, the initial rate of formation of Mg(OH)₂ layer as a corrosion by-product on the fresh surface of Mg is higher. Therefore the change in pH is rapid in the initial hours of immersion. Once the Mg(OH)₂ layer is formed on the surface of Mg, then the corrosion rate is decreased as the Mg(OH)₂ layer acts as a barrier. However, due to the presence of Cl ions, the

Mg(OH)₂ layer is slowly degraded, and Mg corrosion is further increased. Hence, pH change is bigger during the initial hours of the immersion. The pH was found to be stabilized in all the samples with the increased immersion time. Compared with the composites, SBF solution containing pure Mg was observed with marginally higher pH values due to more degradation.

Higher mineral depositions help to delay the degradation process by stabilizing the Mg(OH)₂ phase produced due to bio-corrosion of Mg and also delay the transformation of (Mg(OH)₂ into magnesium chloride [43]. The mineral phases of Ca/P also promote better bonding at the implant-tissue interface [30]. Therefore, a higher rate of biomineralization is always preferred in developing Mg-based implants to achieve lower degradation and a higher rate of healing [44,45]. In the present work, lamellar microstructure and incorporated nano-fHA crystals are the two important factors that played an important role in increasing the biomineralization by which the degradation was decreased. Hence, from the results, it can be summarized that ball milling results in the micro-lamellar structure which is also seen in the sintered Mg-Zn-fHA composites. The added fHA crystals enhanced biomineralization which is favorable for degradable implant applications. The present results encourage future studies with other potential Mg alloys (with biocompatible alloying elements) as matrix material.

4. Conclusions

Composites of Mg-Zn-fish bone-derived hydroxyapatite (fHA) with micro-lamellar morphology were produced with 1% and 2% fHA content by ball milling and sintering. The XRD studies showed no indication of the formation of any new phases after milling. The altered peak intensities indicate basal texture in the milled powders. The ball-milled powders were observed with a flake-like structure, and the same has been retained after sintering and appeared as a micro-lamellar structure. Immersion studies in simulated body fluids indicated better mineral deposition of Ca/P phase on the composites than pure Mg. pH measurements also indicated lower degradation for the composites. Composite with 1% HA was observed with lower weight loss than composite with 2% HA. Hence for the results, it can be concluded that Mg-Zn-1%HA can be a viable composition with a micro-lamellar structure to manufacture Mg-based implants for degradable biomedical implants.

Funding

This research received no external funding.

Acknowledgments

This research has no acknowledgment.

Conflicts of Interest

The authors declare no conflict of interest.

References

1. Nikhilesh, C.; Krishan K.C. *Metal Matrix Composites*. 2nd ed., Springer, New York, **2013**; pp. 37-54, <https://doi.org/10.1007/978-1-4614-9548-2>.
2. Yi, L.J.; Li, J.F.; Ma, M.G.; Zhu, Y.J. Nanostructured Calcium-Based Biomaterials and Their Application in Drug Delivery. *Curr Med Chem.* **2020**, *27*, 5189-5212, <https://doi.org/10.2174/0929867326666190222193357>.

3. Antoniac, I.; Adam, R.; Bitá, A.; Miculescu, M.; Trante, O.; Petrescu, I.M.; Pogarasteanu, M. Comparative Assessment of In Vitro and In Vivo Biodegradation of Mg-1Ca Magnesium Alloys for Orthopedic Applications. *Materials* **2021**, *14*, <https://dx.doi.org/10.3390/ma14010084>.
4. Li, W.; Shen, Y.; Shen, J.; Shen, D.; Liu, X.; Zheng, Y.; Yeung, K.W.K.; Guan, S.; Kulyasova, O.B.; Valiev, R.Z. In vitro and in vivo studies on pure Mg, Mg-1Ca and Mg-2Sr alloys processed by equal channel angular pressing. *Nano Mater. Sci.* **2020**, *2*, 96–108, <https://doi.org/10.1016/j.nanoms.2020.03.004>.
5. Hang, Z.; Bing, Liang.; Haitao, J.; Zhongliang, D.; Kexiao Y. Magnesium-Based Biomaterials as Emerging Agents for Bone Repair and Regeneration: From Mechanism to Application. *J. Magnes. Alloys*. **2021**, *9*, 779–804, <https://doi.org/10.1016/j.jma.2021.03.004>.
6. Shukufe, A.; Masoud, M. Biodegradable Magnesium-Based Biomaterials: An Overview Of Challenges And Opportunities. *Medcomm* **2021**, *2*, 123-144, <https://doi.org/10.1002/mco2.59>.
7. Herber, V.; Okutan, B.; Antonoglou, G.; Sommer, N.G.; Payer, M. Bioresorbable Magnesium-Based Alloys as Novel Biomaterials in Oral Bone Regeneration: General Review and Clinical Perspectives. *J. Clin. Med.* **2021**, *10*, <https://doi.org/10.3390/jcm10091842>.
8. Witte, F.; Hort, N.; Vogt, C.; Cohen, S.; Kainer, K.U.; Willumeit, R.; Feyerabend, F. Degradable Biomaterials Based on Magnesium Corrosion. *Curr Opin Solid St Mater Sci.* **2008**, *12*, 63–72, <https://doi.org/10.1016/j.cossms.2009.04.001>.
9. Rahman, M.; Dutta Naba, K.; Namita, R.C. Magnesium Alloys with Tunable Interfaces as Bone Implant Materials. *Front. Bioeng. Biotechnol.* **2020**, *8*, <https://doi.org/10.3389/fbioe.2020.00564>.
10. Shebeer, A.R.; Muhammad Rabeeh, V.P.; Joseph, M.A.; Hanas, T. Does Acid Pickling of Mg-Ca Alloy Enhance Biomineralization? *J. Magnes. Alloys* **2021**, *9*, 1028-1038, <https://doi.org/10.1016/j.jma.2020.12.002>.
11. Kirkland, N. T.; Birbilis, N. *Magnesium biomaterials design, testing, and best practice*. Springer, New York, USA, **2014**; pp. 1–131, <https://doi.org/10.1007/978-3-319-02123-2>.
12. Zeng, R.; Dietzel, W.; Witte, F.; Hort, N.; Blawert, C. Progress and Challenge for Magnesium Alloys as Biomaterials. *Adv Eng Mater.* **2008**, *10*, B3–B14, <https://doi.org/10.1002/adem.200800035>.
13. Sourav, D.; Sanjay, G.; Roy, M. Recent Developments in Magnesium Metal–Matrix Composites for Biomedical Applications: A Review. *ACS Biomater. Sci. Eng.* **2020**, *6*, 4748-4773, <https://doi.org/10.1021/acsbomaterials.0c00678>.
14. Saberi, A.; Bakhsheshi-Rad, H.R.; Karamian, E.; Kasiri-Asgarani, M.; Ghomi, H.; Omid, M.; Abazari, S.; Ismail, A.F.; Sharif, S.; Berto, F. Synthesis and Characterization of Hot Extruded Magnesium-Zinc Nano-Composites Containing Low Content of Graphene Oxide for Implant Applications. *Phys. Mesomech.* **2021**, *24*, 486-502, <https://doi.org/10.1134/S1029959921040135>.
15. Sandeep Moudgalya, K.V.; Suresh Hebbar, H. Magnesium Based Biocomposites for Biomedical Applications – A Review. *AIP Conference Proceedings* **2020**, 2247, <https://doi.org/10.1063/5.0003896>.
16. de Castro, M.M; Lopes D.R.; Dias, L.V. *Mg-Based Composites for Biomedical Application*. Intech Open, **2021**; <https://doi.org/10.5772/intechopen.95079>.
17. Lin, K.; Chang, J. Structure and Properties of Hydroxyapatite for Biomedical Applications, Editor(s): Michael Mucalo. In: *Hydroxyapatite (Hap) for Biomedical Applications*. Woodhead Publishing Series in Biomaterials, Woodhead Publishing, **2015**; pp. 3-19, <https://doi.org/10.1016/B978-1-78242-033-0.00001-8>.
18. Amaechi, B.T.; AbdulAzees, P.A.; Alshareif, D.O.; Shehata, M.A.; Lima, P.P.d.C.S.; Abdollahi, A.; Kalkhorani, P.S.; Evans, V. Comparative Efficacy of a Hydroxyapatite and a Fluoride Toothpaste for Prevention and Remineralization of Dental Caries in Children. *BDJ Open* **2019**, *5*, <https://doi.org/10.1038/s41405-019-0026-8>.
19. Vivekanand, S.K.; Sudheer, K.; Krishna Prasad, L. Hydroxyapatite—Past, Present, And Future In Bone Regeneration. *Bone and Tissue Regeneration Insights* **2016**, *7*, 9–19, <https://doi.org/10.4137/BTRI.S36138>.
20. Cestari, F.; Agostinacchio, F.; Galotta, A.; Chemello, G.; Motta, A.; Sglavo, M.V. Nano-Hydroxyapatite Derived from Biogenic and Bioinspired Calcium Carbonates: Synthesis and In Vitro Bioactivity. *Nanomaterials* **2021**, *11*, <https://doi.org/10.3390/nano11020264>.
21. Sawada, M.; Sridhar, K.; Kanda, Y.; Yamanka, S. Pure Hydroxyapatite Synthesis Originating from Amorphous Calcium Carbonate. *Sci Rep* **2021**, *11*, <https://doi.org/10.1038/s41598-021-91064-y>.
22. Masakuni, O.; Suguru, S. Microstructural Development of Natural Hydroxyapatite Originated from Fish-Bone Waste through Heat Treatment. *J. Am. Ceram. Soc.* **2002**, *85*, 1315–1317, <https://doi.org/10.1111/j.1151-2916.2002.tb00268.x>.
23. Boutinguiza, M.; Pou, J.; Comesaña, R.; Lusiños, F.; de Carlos, A.; León, B. Biological Hydroxyapatite Obtained from Fish Bones. *Mater. Sci. Eng. C* **2012**, *32*, 478–486, <https://doi.org/10.1016/j.msec.2011.11.021>.
24. Huang, Y.C.; Hsiao, P.C.; Chai, H.J. Hydroxyapatite Extracted From Fish Scale: Effects on MG63 Osteoblast-Like Cells. *Ceram. Int.* **2011**, *37*, 1825–1831, <https://doi.org/10.1016/j.ceramint.2011.01.018>.
25. Santos, M.H.; de Oliveira, M.; de Freitas Souza, P.; Mansur, H.S.; Vasconcelos, W.L. Synthesis Control and Characterization of Hydroxyapatite Prepared by Wet Precipitation Process. *Mater. Res.* **2004**, *7*, 625–630, <https://doi.org/10.1590/S1516-14392004000400017>.
26. Kojima, Y.; Kitazawa, K.; Nishimiya, N. Synthesis of Nano-Sized Hydroxyapatite By Ultrasound Irradiation. *J. Phys.: Conf. Ser.* **2012**, 339, <https://doi.org/10.1088/1742-6596/339/1/012001>.

27. Suchanek, W.L.; Riman, R.E. Hydrothermal Synthesis of Advanced Ceramic Powders. *Adv. Sci. Technol.* **2006**, *45*, 184–193, <https://doi.org/10.4028/www.scientific.net/AST.45.184>.
28. Cho, J.S.; Kang, Y.C. Nano-Sized Hydroxyapatite Powders Prepared by Flame Spray Pyrolysis. *J. Alloy. Compd.* **2008**, *464*, 282–287, <https://doi.org/10.1016/j.jallcom.2007.09.092>.
29. Ratna Sunil, B.; Jagannatham, M. Producing Hydroxyapatite from Fish Bones by Heat Treatment. *Mater Let* **2016**, *185*, 411–414, <http://dx.doi.org/10.1016/j.matlet.2016.09.039>.
30. Suryanarayana, C. Mechanical Alloying and Milling. *Prog. Mater. Sci.* **2001**, *46*, 1–184, [https://doi.org/10.1016/S0079-6425\(99\)00010-9](https://doi.org/10.1016/S0079-6425(99)00010-9).
31. Khanra, A.K.; Jung, H.C.; Yu, S.H.; Hong, K.S.; Shin, K.S. Microstructure and Mechanical Properties of Mg–HAP Composites. *Bull. Mater. Sci.* **2010**, *33*, 43–47, <https://doi.org/10.1007/S12034-010-0006-Z>.
32. Gu, X.; Zhou, W.; Zheng, Y.; Dong, L.; Xi, Y.; Chai, D. Microstructure, Mechanical Property, Bio-Corrosion and Cytotoxicity Evaluations of Mg/HA Composites. *Mater. Sci. Eng. C.* **2010**, *30*, 827–832, <https://doi.org/10.1016/j.msec.2010.03.016>.
33. Ye, X.; Chen, M.; Yang, M.; Wei, J.; Liu, D. In Vitro Corrosion Resistance and Cytocompatibility of Nano-Hydroxyapatite Reinforced Mg–Zn–Zr Composites. *J. Mater. Sci.: Mater. Med.* **2010**, *21*, 1321–1328, <https://doi.org/10.1007/s10856-009-3954-3>.
34. Khalil, K.A.; Almajid, A. Effect of High-Frequency Induction Heat Sintering Conditions on the Microstructure and Mechanical Properties of Nanostructured Magnesium/Hydroxyapatite Nanocomposites. *Mater. Des.* **2012**, *36*, 58–68, <https://doi.org/10.1016/j.matdes.2011.11.008>.
35. Ratna Sunil, B.; Sampath Kumar, T.S.; Uday Chakkingal; Nandakumar, V.; Mukesh D. Nano-Hydroxyapatite Reinforced AZ31 Magnesium Alloy by Friction Stir Processing: A Solid State Processing for Biodegradable Metal Matrix Composites. *J. Mater. Sci. Mater. Med.* **2014**, *25*, 975–988, <https://doi.org/10.1007/s10856-013-5127-7>.
36. Avedesian, M.; Baker, H. *ASM Specialty Handbook: Magnesium and Magnesium Alloys*. ASM International, USA, **1999**.
37. Kevorkov, D.; Pegguleryuz, M. Experimental Study of The Ce–Mg–Zn Phase Diagram at 350°C via Diffusion Couple Techniques. *J. Alloys Compd.* **2009**, *478*, 427–436, <https://doi.org/10.1016/j.jallcom.2008.11.119>.
38. Syam, P.U.; Kondaiah, V.V.; Akhil, K.; Kumar, V.V.; Nagamani, B.; Jhansi, K.; Dumpala, R.; Venkateswarlu, B.; Ratna, S.B. Effect of Heat Treatment on Microstructure, Microhardness and Corrosion Resistance of ZE41 Mg Alloy. *Koroze A Ochrana Materiálu.* **2019**, *63*, 79–85, <https://doi.org/10.2478/kom-2019-0010>.
39. Kokubo, T.; Takadama, H. How Useful is SBF in Predicting in vivo Bone Bioactivity? *Biomaterials* **2006**, *27*, 2907–15, <https://doi.org/10.1016/j.biomaterials.2006.01.017>.
40. Ratna Sunil, B.; Sampath Kumar, T.S.; Uday Chakkingal; Nandakumar, V.; Mukesh, D. Friction Stir Processing of Magnesium – Nanohydroxyapatite Composites with Controlled in vitro Degradation Behaviour. *Mater. Sci. Eng. C* **2014**, *39*, 315–324, <https://doi.org/10.1016/j.msec.2014.03.004>.
41. Saikrishna, N.; Pradeep Kumar Reddy, G.; Balakrishnan, M.; Ravikumar D.; Jagannatham, M.; Ratna Sunil, B. An Investigation on the Hardness and Corrosion Behaviour of MWCNT/Mg Composites and Grain Refined Mg. *J. Magnes. Alloys* **2018**, *6*, 83–89, <https://doi.org/10.1016/j.jma.2017.12.003>.
42. Ratna Sunil, B.; Ganapathy, C.; Sampath Kumar, T.S.; Uday, C. Processing and Evaluating Mechanical Behaviour of Lamellar Structured Degradable Magnesium-Hydroxyapatite Implants. *J. Mech. Behav. Biomed. Mater.* **2014**, *40*, 178–189, <https://doi.org/10.1016/j.jmbbm.2014.08.016>.
43. Witte, F.; Fischer, J.; Nellesen, J.; Crostack, H.-A.; Kaese, V.; Pisch, A.; Beckmann, F.; Windhagen, H. In Vitro and In Vivo Corrosion Measurements of Magnesium Alloys. *Biomaterials*. **2006**, *27*, 1013–8, <https://doi.org/10.1016/j.biomaterials.2005.07.037>.
44. Ho, Y.-H.; Man, K.; Joshi, S.S.; Pantawane, M.V.; Wu, T.-C.; Yang, Y.; Dahotre, N.B. In-Vitro Biomineralization and Biocompatibility of Friction Stir Additively Manufactured AZ31B Magnesium Alloy-Hydroxyapatite Composites. *Bioact. Mater.* **2020**, *5*, 891–901, <https://doi.org/10.1016/j.bioactmat.2020.06.009>.
45. Bakhsheshi-Rad, H.R.; Hamzah, E.; Ying, W.S.; Razzaghi, M.; Sharif, S.; Ismail, A.F.; Berto, F. Improved Bacteriostatic and Anticorrosion Effects of Polycaprolactone/Chitosan Coated Magnesium via Incorporation of Zinc Oxide. *Materials* **2021**, *14*, <https://doi.org/10.3390/ma14081930>.